

Photonics-Based Broadband Microwave Measurement

Shilong Pan, *Senior Member, IEEE, Member, OSA*, and Jianping Yao, *Fellow, IEEE, Fellow, OSA*

(*Technical Review*)

Abstract—Microwave measurement refers to the acquisition of parameters of a microwave signal or the identification of properties of an object via microwave-based approaches. Thanks to the broad bandwidth and high speed provided by modern photonics, microwave measurement in the optical domain can provide better performance in terms of bandwidth and speed which may not be achievable using traditional, even state-of-the-art electronics. In this tutorial, techniques for photonics-based broadband and high-speed microwave measurement are discussed with an emphasis on the system architectures for microwave signal parameter measurement and object property identification. Emerging technologies in this area and possible future research directions are also discussed.

Index Terms—Electromagnetic field measurement, instantaneous frequency measurement, microwave measurement, microwave photonics, phase noise, photonics-based radar, position localization.

I. INTRODUCTION

MICROWAVE measurements are conventionally performed using electronic devices. The advantages of purely electronic microwave measurements include high resolution and high flexibility. For many applications, however, microwave measurements for wideband and high speed signals are needed, which may not be implementable via electronic devices due to the limited speed and bandwidth. On the other hand, modern photonics can provide a much broader bandwidth, which can be used for wideband and high speed microwave measurements. A variety of photonics-based techniques have been proposed and developed in recent years [1]–[6]. In general, photonics-based microwave measurements can be roughly divided into two categories: the measurements of parameters of a microwave signal such as power, phase, phase noise, instantaneous frequency, and spectrum, and the non-contact measurement of the properties of

an object (e.g., position, velocity, and direction of arrival) using microwave as the medium.

To measure the parameters of a microwave signal, the microwave signal to be measured is first converted to the optical domain using a modulator. The microwave-modulated optical signal is then sent to an optical processing module where the parameter to be measured is converted to an amplitude change. The amplitude information is finally extracted with a photodetector (PD). Photonics-based techniques can also be employed to implement broadband microwave signal generation, distribution, and processing, to construct high-performance radar and distributed antenna systems for non-contact measurement of objects.

This tutorial contains an overview of recent photonics-based microwave measurement techniques developed for broadband microwave measurements such as electric field, phase noise, instantaneous frequency, and spectrum. A photonics-based radar and fiber-connected distributed antenna system for position localization are also introduced, and emerging technologies in this area and possible future research directions are discussed.

II. MEASUREMENT OF MICROWAVE SIGNAL PARAMETERS

A. Electric Field Measurement

Electric-field measurement refers to the amplitude measurement of an electrical field, which is of critical importance in fields like high-voltage engineering, electromagnetic compatibility, antenna measurements, non-destructive inspection, and bioelectromagnetism. Conventionally, metallic antennas are used to measure the electric fields. Their considerably large size and metal composition, however, would distort the original electric field, resulting in poor spatial resolution and imprecise measurement [7]. Transient electric fields are particularly difficult to measure with traditional electric-field sensors. On the contrary, electro-optic (EO) sensors are compact and dielectric, which prevents the distribution of the electric field being measured from perturbation and allows for accurate measurement and high spatial resolution. EO sensors also have large enough bandwidth for measuring transient electric fields [8], [9].

The EO sensor is essentially similar to an electro-optical modulator (EOM), which, in most cases, is built based on the Pockels effect in an EO crystal. When performing electric-field measurement, the optical modulation scheme in an EO sensor can be amplitude, phase or polarization state modulation.

Manuscript received June 2, 2016; accepted June 17, 2016. Date of publication July 6, 2016; date of current version June 24, 2017. This work was supported in parts by the National Natural Science Foundation of China under Grants 61527820 and 61422108, the Jiangsu Provincial Program for High-level Talents in Six Areas (DZXX-034), the “333 Project” of Jiangsu Province (BRA2015343), and the Natural Sciences and Engineering Research Council of Canada.

S. Pan is with the Key Laboratory of Radar Imaging and Microwave Photonics, Ministry of Education, Nanjing University of Aeronautics and Astronautics, Nanjing, 210016, China (e-mail: pans@iee.org).

J. Yao is with the Microwave Photonics Research Laboratory, School of Electrical Engineering and Computer Science, University of Ottawa, Ottawa, ON K1N 6N5, Canada (e-mail: jpyao@eecs.uottawa.ca).

Color versions of one or more of the figures in this paper are available online at <http://ieeexplore.ieee.org>.

Digital Object Identifier 10.1109/JLT.2016.2587580

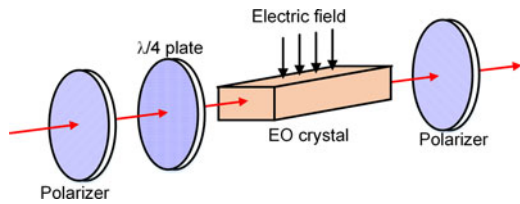


Fig. 1. Diagram of a typical electric-optic sensor. EO crystal: electro-optic crystal.

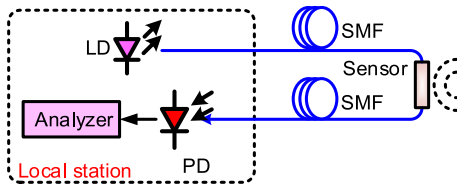


Fig. 2. Diagram of a typical electric-field measurement system. LD: laser diode. PD: photodetector. SMF: single mode fiber.

According to a comprehensive investigation conducted in a previous study [10], amplitude-modulation-based EO sensors perform slightly better than sensors based on either of the other two modulation schemes. Accordingly, optical amplitude modulation is most commonly employed in electric-field measurement systems. Fig. 1 shows a diagram of a typical EO sensor based on optical amplitude modulation. In this system, two polarizers with orthogonal polarization directions are placed at the two ends of a waveguide formed by an EO crystal. To maintain a linear relationship with the applied electric field without a DC bias, a quarter-wave plate is inserted between the first polarizer and the EO crystal to introduce an additional phase shift of $\pi/2$ between the ordinary and extraordinary light waves. When the electric field to be measured is applied, the refraction index of the EO crystal is modified and an amplitude-modulated optical signal is generated at the output of the second polarizer. After converting the modulated optical signal into an electrical signal and detecting the signal in the time (or frequency) domain, the electric field is measured.

Fig. 2 shows a schematic diagram of a typical electric-field measurement system incorporating a single EO sensor. The EO sensor in the detection zone can be placed far away from the local station. Optical fibers are naturally chosen to connect the sensor with the local station. In the local station, a laser diode (LD) is used to provide the probe light, and a PD followed by an analyzer is employed to perform optical-to-electrical conversion to restore the electric-field information. This system configuration facilitates remote electric-field sensing while minimizing potential distortions to the electric field being measured.

To ensure high spatial resolution, the size of the EO sensor, which is closely related to the EO crystal, should be as small as possible. Previous researchers have extensively investigated the effects of various EO crystals [11]. Initially, EO sensors were typically made of potassium dihydrogen phosphate (KDP), bismuth germanium oxide (BGO), or bismuth silicon oxide (BSO). KDP-based EO sensors fell out of favor due to deliquescence and temperature sensitivity, leaving BGO and BSO crystals more common materials for EO sensors; these types of sensors are

typically oversized, however, due to their small EO coefficient (especially when high sensitivity is required). Recently, lithium niobate (LiNbO_3) crystals with a high EO coefficient, wide bandwidth, and high stability have grown more common, which enable compact size and enhance the sensor's sensitivity, dynamic range, and robustness [12], [13]. Benefitting from the small size, LiNbO_3 -based sensors would nearly not distort the electric field being measured and a high accuracy and high spatial resolution measurement can be achieved. For instance, an integrated EO sensor based on a LiNbO_3 crystal was reported [14], by which the electric field with a spatial resolution as small as $500 \mu\text{m}$ was detected.

Measurement bandwidth is also a crucial consideration in designing any electric-field measurement system. Particularly, a large bandwidth is highly desirable for transient electric-field measurements. To date, the detection of an electric field from DC to several GHz is fairly easily achievable [15] and a dynamic range of over 130 dB spreading from $1 \text{ mV/m/Hz}^{1/2}$ to the breakdown electric field in the air can also be achieved [16], [17]. To detect an electric field that is varying at a frequency as high as terahertz, electro-optical devices with a very high response speed should be used. A gallium phosphide crystal was proven suitable for use in THz wave EO sensors because of its 7-THz bandwidth [18]. A zinc telluride crystal was later demonstrated to be spectrally sensitive beyond 3 THz [19]. To detect such a high-speed signal, a terahertz PD is required to extract the electric-field information [20]; unfortunately, such PDs are usually expensive. To avoid the use of a high speed PD, electric-field measurement schemes based on optical frequency down-conversion can be applied. For example, a recirculating frequency shifter based hybrid electro-optic probing system was proposed to expand the instantaneous probing bandwidth [21]. The recirculating frequency shifter generates a wideband optical frequency comb (OFC) with a frequency spacing of Δf , which is modulated by the received microwave signal with a center frequency of f , generating a series of frequency components with frequencies of $f - n\Delta f$ (n is an integer) after the PD. The system has substantial flexibility, with the potential to down-convert THz frequencies to only a few GHz. The electric-field measuring bandwidth can also be enhanced by applying high-even-order harmonic sidebands produced on an optical-carrier probe beam with two cascaded EOMs [22]. With this method, the sensing frequency range can be routinely expanded by at least four times.

Recently, numerous electric-field measurement solutions using new materials (or with new designs) have been effectively demonstrated. A compact EO sensor based on a silicon-organic hybrid modulator driven by a bowtie antenna was proposed [23], where slow-light effects in an EO polymer refilled silicon-slot photonic crystal waveguide, coupled with broadband electric field enhancement provided by the bowtie antenna, are utilized to enhance the interaction between electrical waves and light waves, leading to an ultra large effective in-device EO coefficient over 1000 pm/V , i.e., remarkably high sensitivity. The bowtie antenna integrated on a doped silicon slot photonic crystal waveguides has a broad operational bandwidth with a maximum resonance frequency of 10 GHz. In [24], live-line detection of small defects in a high voltage composite

insulator using a compact electric-field measurement system is demonstrated. The small size (millimeter in transverse dimensions) of the EO sensor allows the measurements of axial and radial electric-field components close to the composite insulator rod and between sheds, which is a great advantage compared to other defect detection methods.

B. Microwave Phase Noise Measurement

Phase noise measurement is becoming increasingly important for the design and evaluation of modern microwave systems and radio frequency (RF) circuits, such as wireless communications systems, radar systems and analog to digital converters (ADCs). In a wireless communications system, oscillator phase noise in the transmitter and receiver would affect both up-conversion and down-conversion, which eventually decrease the signal-to-noise ratio of the demodulated signal and increase the bit error rate [25]. In a radar system, the phase noise of the local oscillator (LO) would limit the range resolution and receiver sensitivity. Especially in a Doppler radar system, a higher oscillator phase noise would require a higher transmitted power to ensure a correct target detection [26]. In ADCs, the phase noise of the sampling signal will induce sampling errors, which also deteriorate the signal-to-noise ratio of the converted digital signal and increase the bit error rate [27].

Mathematically, the output voltage of a microwave signal from a microwave oscillator can be described as

$$v(t) = V_S \sin [2\pi f_0 t + \Delta\varphi(t)] \\ = V_S \sin \left[2\pi f_0 t + \sum_{f_m} \frac{\Delta f(f_m)}{f_m} \sin 2\pi f_m t \right] \quad (1)$$

where V_S is the amplitude of the signal, f_0 is the ideal frequency, and $\Delta\varphi(t)$ is the phase fluctuation. $\Delta f(f_m)$ is the frequency fluctuation away from the carrier frequency f_m . In general, the level of a phase noise is measured by the ratio of the power in one phase modulation sideband P_{ssb} (calculated in 1 Hz bandwidth) at an offset frequency of f_m to the total signal power P_s , i.e.

$$L(f_m) = \frac{P_{ssb}}{P_s} = \frac{\Delta f^2(f_m)}{2f_m^2}. \quad (2)$$

The unit for phase noise is dBc/Hz. In writing (2), we assumed $\Delta f(f_m)/f_m < \pi/6$.

To measure phase noise, which is essential for RF engineers to find the factors that influence the frequency stability and then improve the performance of microwave systems and RF circuits, at least four techniques have been developed [28]: the direct spectrum technique, frequency discriminator method, phase detector technique, and residual method. All four are based on pure electronic devices. The details of these techniques including their advantages, disadvantages, and recent development have been summarized in [28].

For phase noise measurement, the key parameter indicators are the noise floor and measurement bandwidth. However, all the phase noise measurement systems constructed based on pure electronic devices have a noise floor which increases with

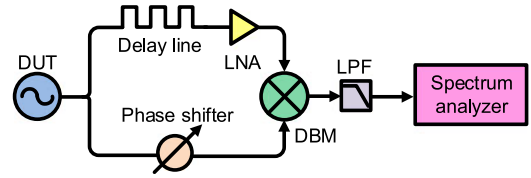


Fig. 3. Phase noise measurement system based on a frequency discriminator. DUT: device under test. LPF: low pass filter. LNA: low noise amplifier. DBM: double-balanced mixer.

frequency. Thanks to this effect, low noise floor and large measurement bandwidth cannot be achieved simultaneously. One approach to mitigate this disadvantage is to replace certain microwave components with their photonic counterparts, as the latter have inherent features including broad bandwidth, low loss, flat frequency response, and high isolation. Previous efforts in this area have led to the successful implementation of the frequency discriminator method in the optical domain.

Fig. 3 shows a typical phase noise measurement scheme based on the frequency discriminator method [29]. The signal from the device under test (DUT) is divided equally into two parts. The first part is delayed by a delay line, through which small frequency fluctuations of the DUT are converted into phase fluctuations. A mixer is used as a phase detector, which converts the phase difference between the two paths into a DC voltage. To maintain phase quadrature of the carrier frequency at the two inputs of the mixer, a phase shifter is inserted in the undelayed path.

The obtained DC voltage at the output of the mixer is related to the phase detector constant K , the fixed time delay τ_d , and the frequency fluctuation of the DUT $\Delta f(f_m)$ by

$$V(f_m) = K2\pi\tau_d\Delta f(f_m). \quad (3)$$

The output voltage is measured by a low-frequency spectrum analyzer as a double sideband voltage spectral density $S_v(f_m)$. According to (2) and (3), $L(f_m)$ is related to the measured $S_v(f_m)$ by

$$L(f_m) = \frac{V^2(f_m)}{8K^2\pi^2\tau_d^2} f_m^2 = \frac{S_v(f_m)}{8K^2\pi^2\tau_d^2 f_m^2}. \quad (4)$$

$S_v(f_m)$ can be read from the spectrum analyzer, the phase detector constant K is calculated by measuring the DC output voltage change of the mixer for a known phase change in one input of the mixer, and τ_d can be calculated by

$$\tau_d = \sqrt{\epsilon_r} \frac{L_d}{c} \quad (5)$$

where ϵ_r is the relative dielectric constant of the delay line, and L_d is delay line deference between the two paths [28]. With the known $S_v(f_m)$, K , and τ_d , $L(f_m)$ can be calculated by (4).

The delay-line frequency discriminator technique is limited by the delay line in two aspects. On one hand, its sensitivity is limited by the loss of the delay-line due to the power requirement of the mixer; using a lower power than that required will degrade the sensitivity. On the other hand, the measurement bandwidth is limited by the bandwidth of the delay line. For instance, NoiseXT PN9000 [30], a commercial phase noise measurement

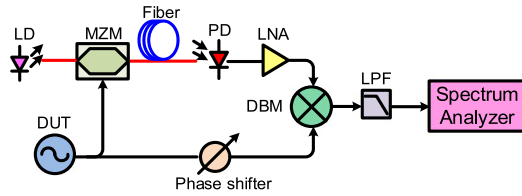


Fig. 4. Phase noise measurement system based on optical fiber delay. MZM: Mach-Zehnder modulator.

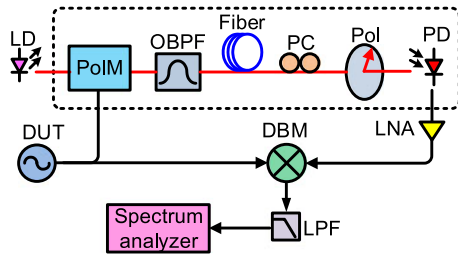


Fig. 5. Phase noise measurement system based on a microwave-photonic phase shifter. PoIM: polarization modulator. OBPF: optical band pass filter. PC: polarization controller. Pol: polarizer.

instrument based on frequency discriminator technique using coaxial cable as the delay line, can only measure a DUT with a frequency ranging from 2 MHz to 1.8 GHz.

In effort to remedy these problems, a phase noise measurement system based on optical fiber delay was established [31], with the schematic diagram shown in Fig. 4. Due to the low loss (~ 0.2 dB/km), large bandwidth (~ 10 s THz) and small signal distortion, the optical fiber is an optimal device to serve as a delay line. The noise floor of this system can reach -130 dBc/Hz at an offset frequency of 10 kHz from a carrier frequency of 10 GHz [32].

It is important to note that the noise floor of the measurement system depends on the length of the optical fiber – the longer the fiber, the lower the noise floor. But a longer fiber also means a higher loss and a lower offset frequency [28]. This problem might be solved by using a longer optical fiber for low-offset-frequency measurement and a shorter delay line for high-offset-frequency measurement [33].

Although using an optical fiber to replace the electronic delay line enhances measurement sensitivity because a much longer delay line can be applied, the measurement bandwidth is still limited by electrical components in the system such as the phase shifter and mixer. To increase the bandwidth, the electrical phase shifter in Fig. 4 can be replaced with a wide-band microwave-photonic phase shifter as shown in Fig. 5 [33]. The photonic components in the dashed box are used to realize electrical-to-optical conversion, time delay, and phase shift. The microwave-photonic phase shifter consists of a polarization modulator (PoIM), an optical bandpass filter (OBPF), a polarization controller (PC), a polarizer, and a PD. Its operation process was described in [34]. By adjusting the PC, the phase of the microwave signal recovered at the PD can be continuously adjusted within a full 360° range. The noise floor of this system is -133 dBc/Hz at an offset frequency of 10 kHz from a

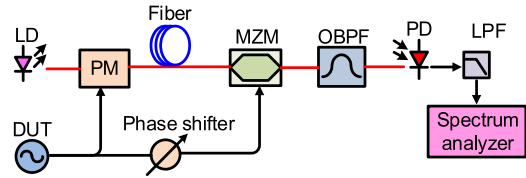


Fig. 6. Phase noise measurement system based on a microwave-photonic frequency down-converter. PM: phase modulator. TOBPF: tunable optical band pass filter.

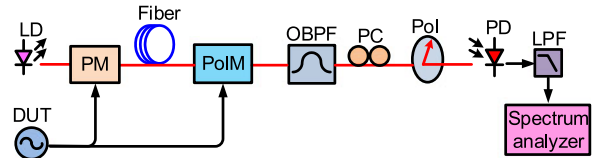


Fig. 7. Phase noise measurement system applying both microwave photonic phase shifter and microwave photonic down-converter.

carrier frequency of 10 GHz, reflecting the fact that the sensitivity of the system is not affected by the microwave-photonic phase shifter. The wide operational bandwidth of the system, from 5 to 40 GHz, is also verified by phase noise measurement of a wideband signal source.

In addition to the phase shifter, active devices including the electronic mixer and low noise amplifier (LNA) also significantly affect the performance of phase noise measurement systems. Accordingly, a phase noise measurement system based on a microwave-photonic frequency down-converter was established [35], as shown in Fig. 6. An EOM is used to convert the microwave signal to be measured to the optical domain, generating an optical carrier and two sidebands. After being time delayed by an optical fiber, the optical signal is modulated by the microwave signal again at a second EOM, generating another pair of sidebands. Frequency down-conversion is realized by selecting two first-order sidebands on one side of the optical carrier and beating them at a PD [36]. The incorporation of the electro-optical mixing in the system not only removes the measurement bandwidth limit by the electronic mixer but also avoids the sensitivity degradation caused by the electrical signal amplification because the nonlinear effect in the EOM is sufficiently strong. The noise floor of such a system can reach -137 dBc/Hz at an offset frequency of 10 kHz from a carrier frequency of 10 GHz, and the measurement range is from 5 to 40 GHz.

Incorporating both microwave photonic phase shifter and microwave photonic mixer in the measurement system, as shown in Fig. 7, all the high-frequency electronic devices can be avoided [37]. This system can achieve a large operation bandwidth, which is limited only by the bandwidth of the EOMs, and phase noise measurement sensitivity as low as -140 dBc/Hz at an offset frequency of 10 kHz from a carrier frequency of 10 GHz.

The measured phase noise through the systems mentioned above consists of the DUT phase noise and the equipment background noise. To further improve the phase noise measurement sensitivity, a two-channel cross-correlation technique

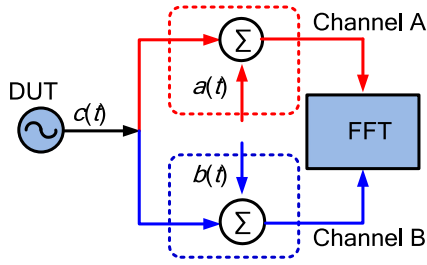


Fig. 8. Two-channel cross-correlation technique for phase noise measurement. FFT: fast Fourier transformation.

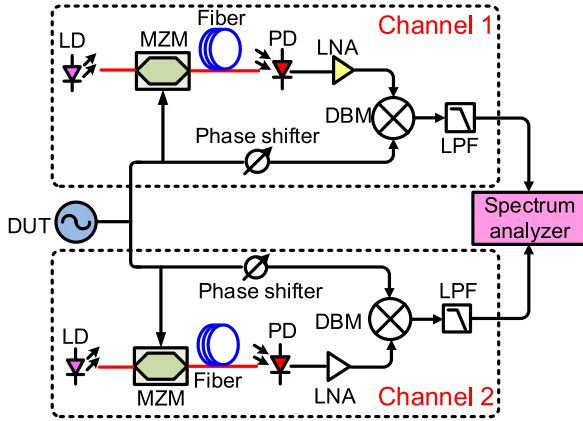


Fig. 9. Two-channel cross-correlation system based on optical delay lines.

can be applied, which can efficiently reduce the equipment background noise [38]. Fig. 8 shows the diagram of a typical two-channel cross-correlation technique. Suppose $A(f)$ and $B(f)$ are the Fourier transforms of the signals in channels A and B, respectively, which can be expressed as

$$A(f) = \text{FFT}[a(t) + c(t)] \quad (6)$$

$$B(f) = \text{FFT}[b(t) + c(t)] \quad (7)$$

where $a(t)$ and $b(t)$ are the uncorrelated equipment background noise that exist in channels A and B, respectively, and $c(t)$ is the DUT phase noise. The cross spectrum of signals in these two channels is defined as

$$S_{AB}(f) = A(f) \times B^*(f). \quad (8)$$

By averaging the cross spectrum S_{AB} , the uncorrelated noise $a(t)$ and $b(t)$ are dramatically reduced. Averaging over m spectra, the uncorrelated noise would decrease by a factor of $1/\sqrt{2m}$ [39]. As a result, the phase noise sensitivity can be improved by increasing the number of correlations.

Fig. 9 shows one implementation of such a technique in the optical domain, with two sets of almost identical components to form two channels [40]. A commercial photonics-based phase noise measurement system released by OEwaves, PHENOM was built based on this configuration [41], which has a noise floor as low as -170 dBc/Hz at an offset frequency of 10 kHz from a carrier frequency of 10 GHz.

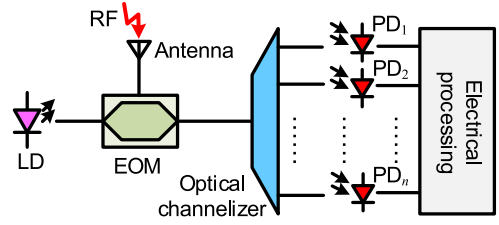


Fig. 10. Microwave spectrum analysis system based on an optical channelizer. EOM: electro-optical modulator.

C. Spectrum Analysis

Cognitive radio and warfare systems must have the capability to estimate the frequency of an unknown input signal over a large spectral range, but the measurement range of the frequency or spectrum measurement system using pure electrical solutions is limited due to the electronic bottleneck. By virtue of the broad bandwidth, photonics-based frequency or spectrum measurement can potentially secure a larger measurement range. In addition, photonics-based measurement technologies also offer advantages such as low loss and immunity to electromagnetic interference (EMI). In recent decades, extensive research has been conducted to the design and implementation of the spectrum measurement of microwave signal based on photonic techniques [42].

Generally, photonics-based microwave spectrum measurement techniques can be classified into two main categories. In the first category, an optical channelizer is employed to spectrally divide the microwave modulated optical signal into contiguous parallel channels [43]–[46]. The optical spectrum of the optical microwave signal is obtained by detecting the optical signals in each channel. In the second category, optical spatial-spectral material is applied to analyze the spectra of broadband or frequency agile microwave signals [47]–[49].

1) *Spectrum Measurement Via an Optical Channelizer*: A conceptual diagram of the microwave signal spectrum measurement scheme based on an optical channelizer is shown in Fig. 10. The microwave signal is first converted into an optical signal using an EOM, then the optical microwave signal is split into various contiguous parallel channels with the optical channelizer. Each channel corresponds to a particular microwave frequency. The split optical signals are then detected by an array of PDs and finally sent to an electrical processing unit to obtain the spectral information [42]. The key component in the system is the optical channelizer, which is effectually an array of narrowband optical filters with adjacent pass bands. Previously, the optical channelizer was realized by an integrated optical phased array consisting of multiple electro-optic waveguide delay lines [43], a high-resolution free-space diffraction grating [44], an array of phase-shifted fiber gratings [45], and an integrated Bragg-grating with a Fresnel lens [46]. A review of these optical channelizers can be found in [42]. Although the optical channelizer can support spectrum measurement of microwave signal with a large bandwidth, its resolution is limited by the minimum achievable bandwidth of the optical filter array (typically larger than 1 GHz) which must have precise center

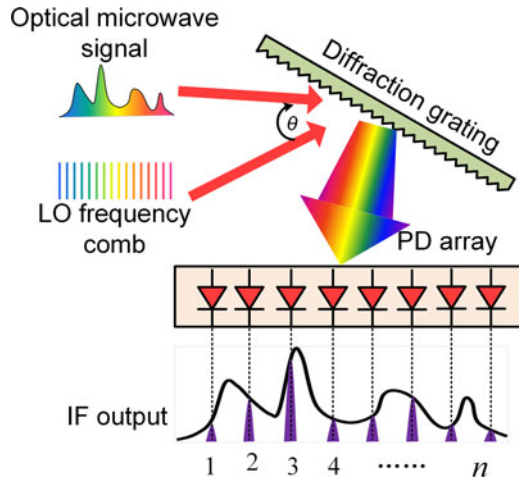


Fig. 11. Diagram of the microwave spectrum analysis system based on coherent optical channelizer using a diffraction grating.

frequencies and identical bandwidth. One solution to this problem is the coherent channelization implemented based on OFCs [50]–[52], which can theoretically realize kHz-level resolution.

Fig. 11 shows one of the earliest coherent optical channelizer proposed by W. Wang *et al.* [44]. The light wave modulated by the microwave signal to be measured is incident to a diffraction grating. Different frequency components are dispersed with different angles and subsequently directed onto a detector array, and the position of the detector corresponds to a particular microwave frequency. An OFC with a frequency spacing equal to the channel spacing is incident to the grating at an offset angle with respect to the optical microwave signal, so every portion of the signal spectrum is translated to the same IF band and each channel can use the same post-processing electronics, which greatly reduces the complexity of the processing system. This approach, however, still has a limited resolution due to the necessity of narrowband filtering (which is determined by the resolution of the diffraction grating and the position of the detector).

To overcome this problem, the single-frequency laser source in Fig. 10 can be replaced by an OFC and the optical channelizer is changed to a periodic optical filter (e.g. Fabry-Pérot filters [50]) together with a wavelength-division multiplexer (WDM). The OFC is modulated to create an array of copies of microwave signal. Then, the periodic optical filter with a free spectral range (FSR) that differs slightly from the wavelength spacing of the OFC is employed to select different frequency components in the RF copies around different comb lines. Finally, the WDM splits the selected frequency components around different comb lines into different channels.

However, the wavelength drift of the periodic optical filter or the optical microwave signal will seriously affect the performance of the optical channelizer containing a periodic optical filter. To remedy this, coherent channelization using two coherent OFCs with slightly different wavelength spacings can be applied. Fig. 12 illustrates the operation principle. The microwave signal to be measured is copied by an OFC in the optical domain and each copy is coupled with a comb line of a local OFC and directed to a spatially separated channel by

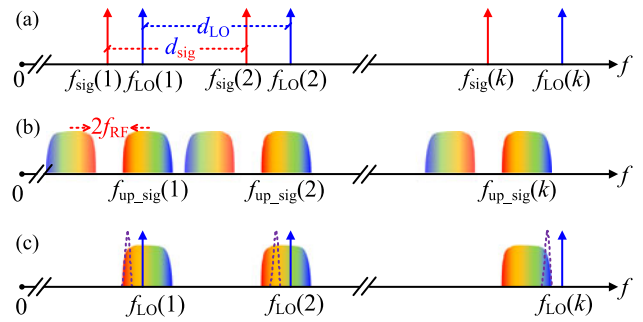


Fig. 12. Optical channelization based on dual coherent OFCs. (a) The signal OFC and local OFC. (b) The modulated signal OFC. (c) Extracting different spectrum slices of the microwave signal in each channel. OFC: OFC.

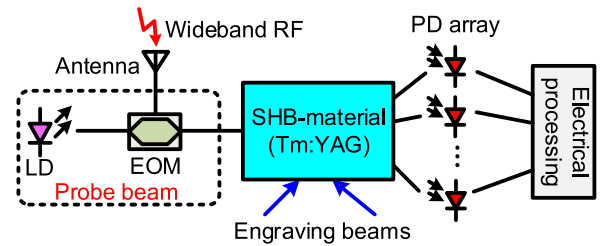


Fig. 13. Spectrum analyzer based on spatial-spectral material with an engraving laser. SHB: spectral hole burning.

a WDM. Via the optical-to-electrical conversion in a PD and low-pass or bandpass filtering in an electrical filter, different components in the microwave signal are selected and presented in different channels. Wavelength drift is not a problem because the two OFCs can be generated using the same seed laser, and because the WDM has relatively broad passbands which can tolerate certain wavelength drifts. Typical coherent optical channelizer based on dual coherent OFCs were demonstrated in [51], [52], which demonstrated that microwave spectrum analysis with high frequency resolution and high crosstalk suppression is, in fact, achievable.

2) *Spectrum Measurement Via Spatial-Spectral Material:* The key component of the spatial-spectral material based spectrum measurement is a rare earth doped material which can be used to record the power spectrum of an optical signal under the spectral hole burning (SHB) effect. The individual ions in the rare earth doped crystal have narrow optical resonances, exhibiting linewidths in the kilohertz order at cryogenic temperatures (4–6 K). The inhomogeneous absorption profile can range from 20 to over 200 GHz, which provides a natural advantage for broadband spectrum measurement. There are generally two types of spatial-spectral material based spectrum analysis techniques: the use of an engraving laser or the use of a linear chirped reading out laser.

Fig. 13 shows a schematic diagram of the spatial-spectral material-based microwave spectrum analyzer with an engraving laser [53]. In the spatial-spectral material, two monochromatic angled beams from the engraving laser inscribes an absorption grating based on SHB effect, which is able to diffract the incident probe beam. The microwave signal to be analyzed is modulated onto an optical carrier, serving as the probe beam, which is tuned to the resonance wavelength of the ions (Tm 793 nm or

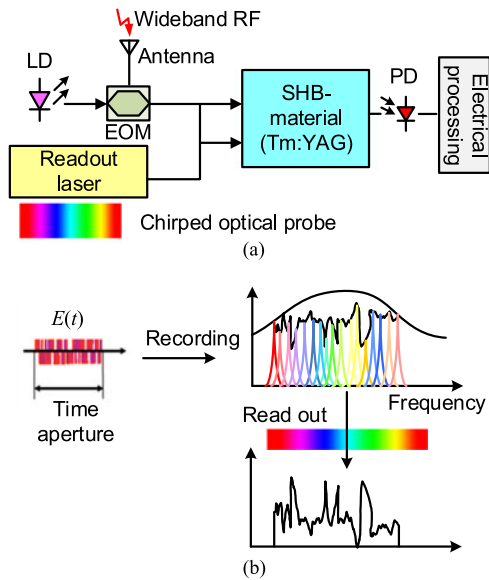


Fig. 14. Spatial-spectral material based spectrum analyzer with a linear chirped laser. (a) Schematic diagram. (b) Operation principle.

Er 1.5 μm) with a large-bandwidth EOM. By scanning the engraving laser frequency in synchrony with the angle of incidence during the grating engraving procedure, different spectral components of the input light beam are diffracted in different directions; the spectrum information is then recorded using a PD array. Due to the complexity of the scanning engraving laser and PD array, this technique is very difficult to be implemented in practice. In addition, its response speed is quite low.

To solve the problems described above, a spatial-spectral material based spectrum analysis technique using a linearly chirped reading out laser was proposed [47]. The principle of this type of technique is illustrated in Fig. 14. First, the modulated optical beam illuminates one spatial location on the spatial-spectral crystal. When the bandwidth of the modulated optical beam lies within the inhomogeneous absorption profile of the material, the full power spectrum of the optical beam is recorded through the optical SHB effect. Multiple frequencies can be burned independently and simultaneously, where the absorption depth depends on the power at each frequency. This recorded power spectrum stored in the modified absorption profile can persist for the population lifetime of the absorption transition levels, which is about 10 ms in Tm- and Er-doped crystals [47]. A linear frequency chirp laser is used to read out the spectrum stored in the spatial-spectral material, as shown in Fig. 14(b). The output field is the time domain map of the recorded spectrum while the transformation between the coordinate domains is scaled by the chirp rate, so the broadband spectrum information can be read out using a low-frequency oscilloscope when the chirp rate is sufficiently slow. For instance, by using a linear chirped laser with external modulation, the response time is improved to the millisecond [48], [54]. The measurement resolution can reach 1 MHz in a measurement range of 10 GHz. Because the chirped laser generation system is always not ideal, a spectroscopic technique can be employed, which can achieve spectral analysis covering a bandwidth of 10 GHz with >5500 spectral

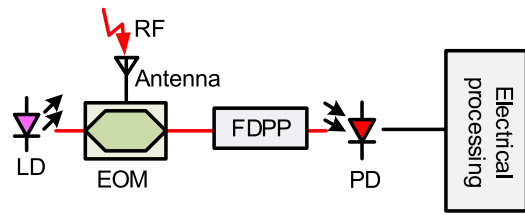


Fig. 15. Microwave frequency measurement system based on microwave power monitoring. FDPP: frequency-dependent power penalty.

channels and 43-dB dynamic range [49]. In addition, fine resolution and broad bandwidth can be achieved simultaneously by using an enhanced chirped fiber laser [55].

The key advantages of the spectrum measurement technology based on the SHB effect in spatial-spectral material is that the spectra of the microwave signals can be analyzed with broad bandwidth, high spectral resolution, large dynamic range, and low readout latency [47], [56], but the disadvantage is also evident include the fact that the SHB effect is significant only if the spatial-spectral material is cryogenically cooled.

D. Instantaneous Frequency Measurement

Instantaneous frequency measurement (IFM) is an important task in radar warning receivers, antistealth defense, and electronic intelligence systems. Fast measurement speed, accurate measurement, and large frequency measurement range are essential for these applications. Unfortunately, conventional electrical IFM systems are vulnerable to EMI and usually have measurement range limited to about 18 GHz due to the limited bandwidth of the electronic components. Microwave photonic techniques can be employed to extend the bandwidth of IFM receivers to tens or even hundreds of GHz, and also offer the advantage of immunity to EMI.

For the IFM, as compared to the spectrum analysis, we need not to know the detailed spectrum of the microwave signal, so the measurement can be significantly simplified while the measurement resolution and range are evidently improved. Generally, photonics-based IFM can be implemented by monitoring microwave power, optical power, or time delays since a fixed relationship between the microwave frequency and the microwave power, optical power or time delay can be established in the optical domain.

1) *IFM Based on Microwave Power Monitoring:* A typical IFM scheme based on microwave power monitoring is shown in Fig. 15 [42]. The unknown microwave signal is first converted at an EOM into an optical microwave signal consisting of two sidebands and an optical carrier (DSB+C), then the optical microwave signal is inserted into an optical channel that can induce a frequency-dependent power penalty. Beating the optical carrier with the upper sideband and the lower sideband at a PD would generate a new microwave signal of which the power, as compared to the original power of the microwave signal, is a function of the microwave frequency. To eliminate the effect of power fluctuation produced by the measurement system two parallel measurements using two optical channels with different frequency-dependent power penalties are usually required.

TABLE I
PERFORMANCE OF IFM TECHNIQUES BASED ON MICROWAVE POWER MONITORING

Techniques	Measurement range (GHz)	Measurement error (GHz)
IM + CD [57]	4–12	±0.1
IM + CD [58]	5–15.6	±0.1
PM + CD [59]	7.3–17.95	±0.5
IM + CD, assisted by electronic pre-processing [60]	4–19	±0.1
IM/PM+CD [61]	2–19	± 0.2
PolM+CD [62]	3–18	± 0.2
Photonic microwave filter pair [63]	0.5–36	±0.2
Single-passband photonic microwave filter [64]	0.4–1.6	±0.06
IM/PM + CD [65]	0.5–20	±0.09
PolM + CD [66]	2–20	±0.1
IM + CD + FWM [67]	0.04–40	±0.1

IM: intensity modulation; PM: phase modulation; PolM: polarization modulation; PolM: polarization modulation; CD: chromatic dispersion; FWM: four-wave mixing.

The ratio of the microwave powers in the two measurements is defined as the amplitude comparison function (ACF). If the ACF has a monotonic relationship with the frequency of the microwave signal in a certain frequency range, IFM can be realized without ambiguity. To form such monotonic relationship, the frequency-dependent power penalties can be realized using a dispersive element or a photonic microwave filter.

When the frequency-dependent power penalty is realized by a dispersive element, the power of the microwave signal from the PD is a function of the chromatic dispersion (CD) and the microwave frequency. To realize two different frequency-dependent power penalties, different dispersion values or different modulation schemes can be applied. The former method can only provide IFM with a limited measurement range, since the ACF at low frequencies has a slow-increasing slope, while the latter can realize IFM with a significantly large measurement range. The microwave frequency response of the system is low pass for an intensity-modulated optical signal transmitting in the dispersive medium, while for a phase-modulated optical signal the frequency response is band pass. Accordingly, the ratio of the two frequency responses has a very steep slope at low frequencies due to the complementary nature of the two frequency responses. Because the measurement range can be extended using a complementary frequency response, a photonic microwave filter with complementary frequency response can also be designed for IFM with a broad measurement range.

A wealth of IFM schemes based on the above methods have been proposed and the performance is summarized in Table I, which shows that the measurement range of this IFM technique can reach 40 GHz and the measurement error is within about ±0.1 GHz.

2) *IFM Based on Optical Power Monitoring*: The major problem associated with conducting IFM by monitoring the microwave power is that it requires high-frequency PD and microwave devices. To avoid the use of these expensive devices, it is possible to create a monotonic relationship between the frequency of the microwave signal to be measured and the optical power, because optical power meter is very cheap. Fig. 16(a)

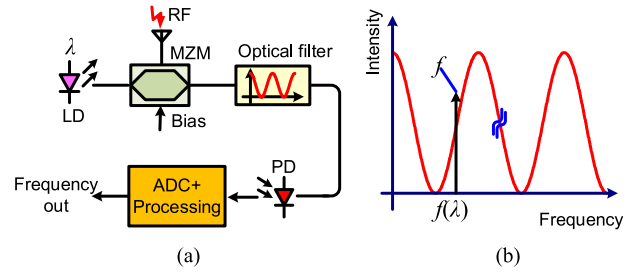


Fig. 16. Microwave frequency measurement system based on optical power monitoring. (a) Schematic diagram. (b) Operation principle.

TABLE II
PERFORMANCE OF IFM TECHNIQUES BASED ON OPTICAL POWER MONITORING

Techniques	Measurement range (GHz)	Measurement error (GHz)
Two-tap Sagnac-loop filter [74]	0–20	±0.2
Integrated ring-assisted Mach-Zehnder interferometer [75]	5–15	±0.2
Complementary polarization domain interferometer [76]	2.5–30 except 16–17.5	±0.5
FBG-based Linear filter [68]	1–10	±0.2
Silicon microdisk resonator [77]	9–19	±0.2
On-chip FWM [78]	0–40	±0.318

illustrates the schematic diagram of a typical microwave frequency measurement system based on optical power monitoring. The microwave signal is converted to an optical signal using a MZM while an optical filter with a special spectral response is placed at the output of the MZM. The wavelength information is thus converted to optical power information. The key component in Fig. 16(a) is the optical filter with sinusoidal spectral response, which can be realized by a two-tap Sagnac-loop filter, an integrated ring-assisted Mach-Zehnder interferometer, and a complementary polarization domain interferometer pair with a tunable FSR. In [68], a specially-designed fiber Bragg grating (FBG) with two spectral slopes inversely proportional to the optical frequency was applied where the ACF is linear with microwave frequency, which ensured the slope of the ACF is the same for different frequencies. In addition to the above techniques, several new IFM techniques based on optical power measurement achieved by on-chip four-wave mixing (FWM) or silicon microdisk resonator were proposed. The performance of these IFM techniques are summarized in Table II.

There are also other photonics-based IFM solutions, such as IFM using a Fabry-Perot scanning receiver [69], photonic Hilbert transform [70], frequency-to-time mapping [71], [72], and nonuniform optical undersampling [73]. Although photonics-based IFM has attracted a great deal of research interest, there is still quite a lot of work to be done to make the techniques practicable. Among various photonic-based IFM techniques mentioned above, the measurement range is typically less than 20 GHz, which does not meet the requirements of modern practical applications. In addition, the measurement error or measurement resolution is generally tens or hundreds of MHz, which is much larger compared to that of electronic

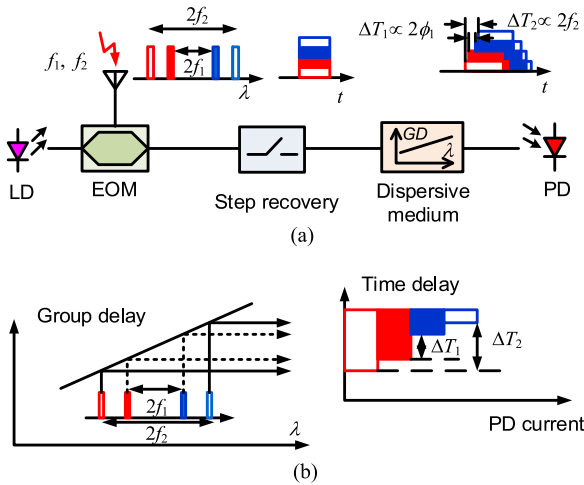


Fig. 17. Multiple-frequency measurement based on frequency-to-time mapping in a dispersive element. (a) Schematic diagram. (b) Operation principle.

schemes. Last but not least, the sensitivity and dynamic range of the IFM system is reduced due to the electrical-to-optical and optical-to-electrical conversion, which must be improved to meet the requirement for working in the realistic electromagnetic environment.

3) *Multiple-Frequency Measurement Based on Frequency-to-Time Mapping*: The majority of the methods discussed above can only be applied for single frequency measurement. In a practical system, however, (such as an electronic warfare system,) various unknown frequency components exist in the received signal. An IFM capable of measuring multiple frequencies is highly desirable, to this effect. Frequency-to-time mapping is an effective approach to achieve simultaneous multiple-frequency measurement. The key point of this method to establish a relationship between the frequency of the unknown signals in the frequency domain and the electrical time delay in the time domain. This relationship can be constructed based on dispersion-induced time delay [71] or frequency shifting recirculating delay line (FS-RDL) [72], [79].

Fig. 17(a) shows a schematic diagram of the multiple-frequency measurement system based on frequency-to-time mapping in a dispersive element [71]. The unknown multiple-tone signals are converted into an optical microwave signal in an EOM using carrier-suppressed DSB (CS-DSB) modulation. A high speed optical on-off switch is used to gate the optical signal, which introduces sharp leading edges as necessary to serve as time measurement reference points. The optical CS-DSB signal is then sent to a PD after being transmitted through a dispersive element with a linear group delay (e.g., chirped-FBG). It is well known that different optical wavelengths would undergo different time delays due to the CD. Therefore, each sideband is mapped into a distinct time slot, as illustrated in Fig. 17(b). Based on this method, in [71] two simultaneous signals at 20 and 40 GHz were measured. It should be noted that although this method can support multiple-frequency measurement, it has a relatively low resolution (~ 12.5 GHz) and a large measurement error (about ± 1.56 GHz), or requires special

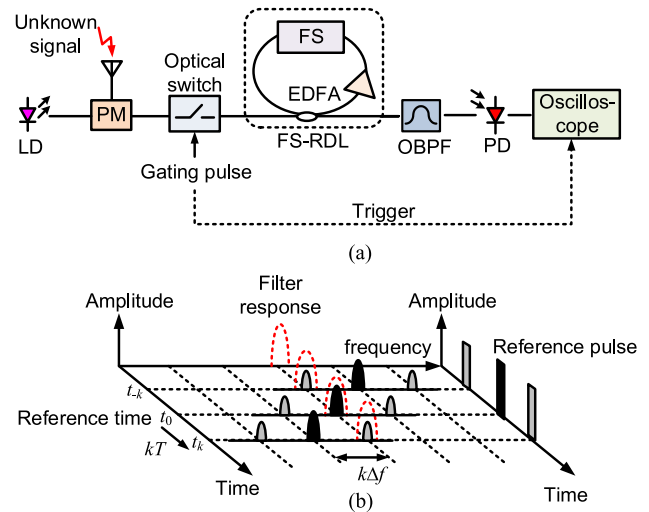


Fig. 18. Multiple-frequency measurement based on a FS-RDL. (a) Schematic diagram. (b) Operation principle. FS: frequency shifter. RDL: recirculating delay line.

capability to acquire the needed relative time delays from the resultant waveform.

Frequency-to-time mapping based on FS-RDL can also be used for multiple-frequency measurement [72]. Fig. 18(a) shows the schematic diagram of a typical multiple-frequency measurement scheme based on an FS-RDL. An optical carrier from an LD is modulated by the unknown microwave signal at a phase modulator (PM), then the phase-modulated optical signal is time-gated by a high-speed on-off optical switch before being launched into an FS-RDL loop. The FS-RDL, as shown in the dashed box in Fig. 18(a), consists of an optical frequency shifter and an optical amplifier. The output of the FS-RDL loop is connected to a narrowband OBPF. The optical signal from the OBPF is detected by a PD, and the obtained photocurrent is observed on a low-frequency oscilloscope that is synchronized with the control pulse connected to the optical switch.

The principle of the frequency measurement system based on FS-RDL is illustrated in Fig. 18(b). Due to the small signal modulation, we assume that the output of the optical switch contains only three optical spectra components: the upper sideband, the optical carrier, and the lower sideband. This signal is injected into the FS-RDL loop. After each circulation, a frequency down-shift of Δf is introduced. After a certain number of circulations, the down-shifted signal would drop in the passband of the OBPF (see the dashed profile). If the OBPF bandwidth is narrow enough, only one optical component is selected at a time, resulting in a square pulse being displayed on the oscilloscope. Corresponding to the relative locations in the optical spectrum, three pulses show up on the oscilloscope sequentially at the time t_{-k} , t_0 , and t_k . To avoid ambiguity, the trigger of the oscilloscope is adjusted to only display the pulse from the upper sideband. Because the frequency shift is related to the time delay when circulating in the FS-RDL, the frequency of the microwave signal can be calculated by measuring the time gap between the pulse for the carrier and that for the upper sideband.

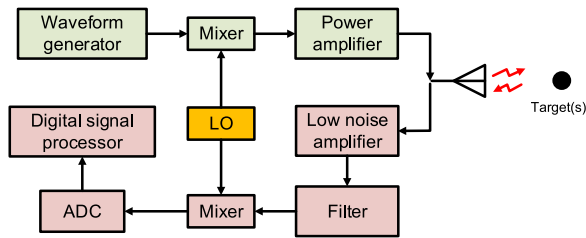


Fig. 19. Typical radar system. LO: local oscillator; ADC: analog-to-digital converter.

Based on this principle, in [72] the OBPF is realized by the in-fiber stimulated Brillouin scattering (SBS) effect which usually results in a passband as narrow as tens of MHz, and therefore a multiple-frequency measurement system with a frequency range of 0.1–20 GHz and a measurement resolution of 250 MHz was demonstrated. In [79], an optical heterodyning scheme and a low-bandwidth PD were applied for the purpose of multiple-frequency measurement, in which one of the optical sidebands of the CS-DSB-modulated signal is down-shifted by the FS-RDL and then directed to the PD in tandem with the optical carrier. When the frequency of the beat signal falls into the PD response window, an electrical pulse can be observed on the oscilloscope. The number of circulation can be counted accurately based on the time of the pulse on the oscilloscope—so the frequency of the unknown signal can be calculated if the frequency shift Δf of the FS-RDL is known.

Due to the fast development of the photonic integration technique, photonic integrated chips (PICs) for IFM applications have garnered sizable research interest. PICs can reduce the size and complexity of the system while enhancing its stability. For instance, if the FS-RDL can be implemented by a PIC, the loop length would be dramatically reduced and thus the response time of the entire system can be reduced. Recently, a Si_3N_4 -based chip [80] and an As_2S_3 -based SBS chip [81] have been proposed for photonics-based microwave frequency measurement.

III. MEASUREMENT USING PHOTONICS-BASED MICROWAVE TECHNIQUES

Different from the measurement of parameters of microwave signals, in which optical methods are mainly used to convert the parameter to be measured into an optical or microwave amplitude/time change, in the photonics-based measurement system for non-contact acquisition of objects' properties, photonics-based techniques are employed to realize broadband microwave signal generation, distribution, or processing. Typical systems in this category includes photonics-based radars and fiber-connected distributed antenna systems.

A. Photonics-Based Radar

Radar is one of the most important measurement systems which uses the microwave as a medium. The basic system block diagram of a radar is shown in Fig. 19. By transmitting microwave signals and analyzing echo parameters such as power, delay, direction and frequency, radar systems can

provide the information on the distance, velocity, position, and electromagnetic scattering characteristics of targets, and can even image the area under radiation. In recent decades, radar systems have gradually put forward the demand for broadening both the instantaneous bandwidth and the working frequency range. With pulse compression technology, the range resolution of a radar system transmitting a waveform of bandwidth B is given by $\delta_r = c/(2B)$ [82]. Thus, for a synthetic aperture radar with a resolution requirement as high as 0.1 m, a microwave waveform with an instantaneous bandwidth of 1.5 GHz is needed. The generation, transmission, receiving and processing of such a broadband signal are challenging for pure electronics based approaches. In addition to the instantaneous bandwidth, a frequency range covering tens of GHz is also required to meet the tendency of multi-band, multi-function and high-density integration in the development of modern radar systems. Again, RF frontend based on pure electronic technology can hardly achieve satisfactory performance over the entire frequency range necessary.

Photonic technologies allow the generation and processing of broadband microwave signals to be implemented in the optical domain, where the optical carrier with a center frequency of up to several hundreds of terahertz can dramatically compress the relative bandwidth of the microwave signal so that the broad-bandwidth related problem in the microwave domain can be effectually eliminated. By applying optical devices with low loss, light weight and immunity to EMI, performance of many important functional units in the radar system can be noticeably enhanced. For instance, with a high-Q optical storage element such as a length of fiber, an optoelectronic oscillator (OEO) can perform as an LO with ultra-low phase noise at a frequency even up to 40 GHz. Microwave signals with an instantaneous bandwidth as large as several octaves can also be directly generated in the optical domain, which could negate the demand for complicated frequency multiplication or up-conversion in the electrical domain. In the receiver, photonic microwave filtering can provide cross-band tunability to enable reconfigurability of the receiver. In addition, ultra-stable pulses from a mode-locked laser (MLL) can be employed to implement photonic-assisted sampling, which can enable high effective number of bits in quantization especially for a high input frequency up to tens of GHz. Moreover, a phased-array radar with a phase shifter-based beamforming network would suffers from the beam squint problem when feeding or receiving a broadband signal. But if the phase shifters are replaced by optical true time delay modules, broadband beams would be properly formed and steered. More details of the advances in the application of photonic technologies in radar can be found in [4], in which many exciting topics, such as OEOs, stable RF signal transfer, microwave photonic filtering, arbitrary waveform generation, beamforming, photonic mixing, phase coding, switching, and ADC, are reviewed at length.

Several photonics-based radar systems have been developed recently [83]–[87]. In [83], a radar capable of measuring both the position and velocity of a target was established with a photonics-based transceiver supporting a broad frequency range up to 40 GHz. As shown in Fig. 20, both the RF generation and the ADC are implemented with the assistance of photonics.

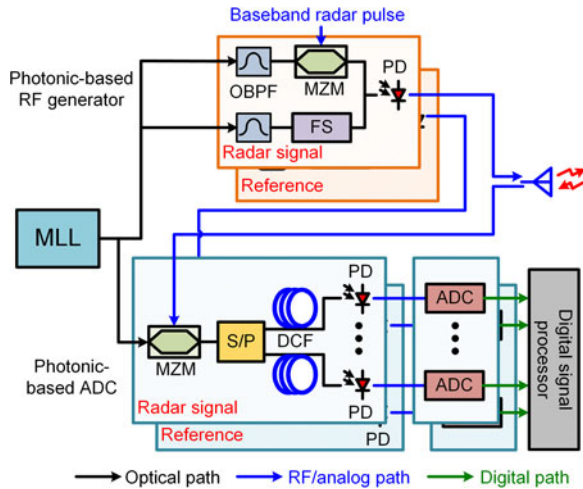


Fig. 20. Radar system based on photonic-based RF generator and photonic-based ADC. S/P: series-to-parallel converter. DCF: dispersion compensation fiber FS: frequency shifter.

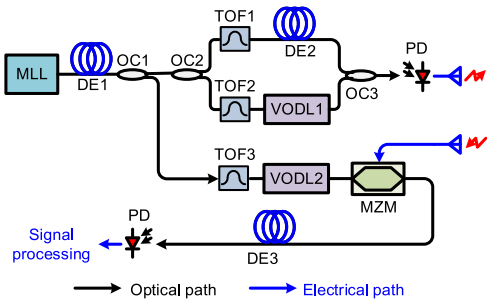


Fig. 21. Photonics-based radar system in [87]. DE: dispersion element; OC: optical coupler; TOF: tunable optical filter; VODL: variable optical delay line.

Furthermore, the mode-locked laser, which provides abundant modes in the optical spectrum, is shared by both the transmitter for RF generation and the receiver for ultra-short sampling so that the coherence of the radar system is ensured. Remarkable enhancements can be found in the operational frequency range and the effective number of bits of ADC at high frequencies. A field-trial demonstration was also conducted to verify the effectiveness of the photonics-based transceiver in the radar system, where velocity resolution of 2 km/h was realized along with a 150-m range resolution, which can be further improved to 23 m via pulse coding. In [84], a photonic radar transceiver capable of simultaneous and independent operation in both X- and S-bands was designed and evaluated. To generate microwave signals with different carrier frequencies, the whole optical spectrum of the pulses from the MLL is intensity-modulated by the IF waveforms so that microwave signals in various bands can be obtained through the beating of MLL modes with disparate spectral spacing. The desired microwave signals are selected from the PD current by microwave bandpass filters and then power-amplified for transmission. In the receiver, photonic bandpass sampling is also implemented and the sampling-induced aliasing helps to down-convert RF signals to their original IFs. This improved system is evaluated in both aerial [85] and maritime scenarios [86]. Because of the coherence of the two bands, the fusion process of data from X- and S- bands for a doubled resolution can be greatly

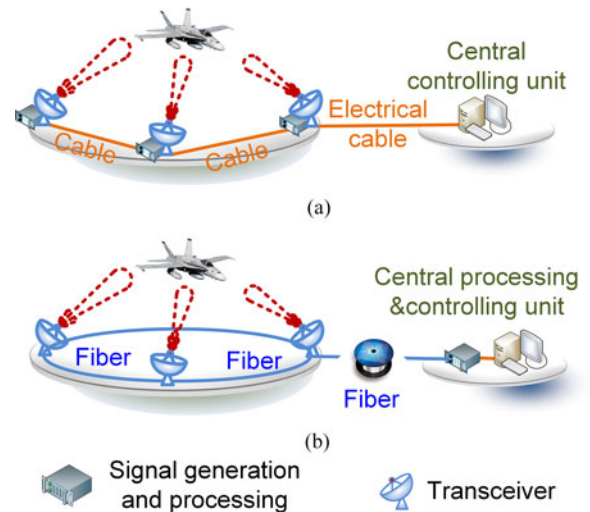


Fig. 22. (a) Conventional distributed radar system. (b) Fiber-connected distributed radar system.

simplified [86]. With the photonic technologies, the schemes in [83]–[86] have remarkably enlarged the carrier frequency range of the radar system. However, the instantaneous bandwidth is still limited to several hundreds of Megahertz because the baseband signal is generated in the electrical domain. Recently, a photonics-based radar system with an instantaneous bandwidth of several GHz was proposed [87], as shown in Fig. 21, in which the transmitted signals are directly generated in the optical domain. To process the broadband signals in the receiver, the large instantaneous bandwidth is compressed in the optical domain through time-stretching in dispersive elements so that a low-frequency electronic ADC can effectively digitize the echo signal. In a dual-target detection experiment, a range resolution of less than 5.7 cm is achieved with a 4-GHz bandwidth X-band signal.

It is worth mentioning that although the photonic-based radar has obvious advantages over traditional radar system in regards to bandwidth and many other aspects, even state-of-the-art photonic technology does not offer a fully workable solution to high-power microwave amplification, which is one of the most important segments in both the transmitter and receiver of a radar system. In addition, the extra loss in optical-to-electrical and electrical-to-optical conversion could also degrade the performance of the entire system. Therefore, the photonic-based radar should not reject the advances in electronic technology and extensive efforts are still required to the development of photonic devices and subsystems so that a promising future of photonic broadband radar can be truly guaranteed.

B. Fiber-Connected Distributed Radar System

Because of the capability of counter-stealth and the significant increase of radar coverage area and angle resolution, distributed radar systems with multiple transceivers have received great interests in the past decades, which can obtain the target information from multiple perspectives [88]–[90]. Conventionally, radar transceivers and the central controlling units in distributed radar systems are connected by electrical cables [91] or wirelessly [92], as depicted schematically in Fig. 22(a). Because

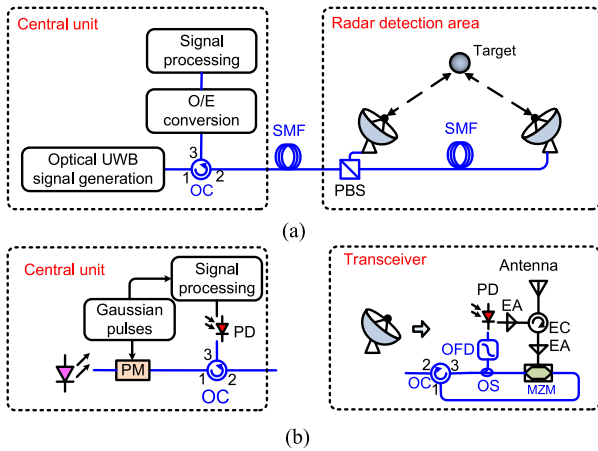


Fig. 23. Fiber-distributed UWB radar network based on wavelength reusing transceivers. OFD: optical frequency discriminator. EC: electrical circulator.

these transmission media always have a relatively small bandwidth (or severe multipath fading) and substantial loss, radar signal generation and received echo processing must be performed in each individual transceiver. To make the cost and the complexity of the transceiver reasonable, only very simple signal processing algorithm can be adopted, inevitably sacrificing the performance of the entire system. In addition, clock synchronization among the transceivers is complicated and usually inaccurate, which further degrades the performance of the radar system.

These limitations can be mitigated by replacing the electrical cable with optical fiber [93], [94]. With the low loss optical fiber as the transmission medium, the radar signals can be generated via a photonic-based approach in a central office (CO), delivered to each radar transceiver by low-loss optical fiber, and processed cooperatively in the CO as illustrated in Fig. 22(b). In at least three aspects, microwave photonic technologies can bring improvement to the distributed radar system: 1) Prolonging the baseline between each pair of transceivers, which increases both the localization accuracy and coverage area; 2) allowing for more sophisticated hardware and software resources by moving the radar signal generation and processing from the transceivers to the CO, which facilitates higher radar performance; and 3) greatly simplifying the transceiver, thus reducing the complexity and cost of the entire system.

Recently, a number of fiber-connected distributed radar systems were developed. In [95], a fiber-distributed bistatic ultra-wideband (UWB) radar based on optical time division multiplexing (OTDM) was reported, as shown in Fig. 23. This radar consists of a CO and two spatially separated transceivers. OTDM technology is implemented by inserting an appropriate length of optical fiber between the two radar transceivers, allowing the UWB pulses received by different transceivers to be identified by the time slots in which they are presented. The UWB pulses emitted from different transceivers are designed to have opposite polarities, allowing the user to readily identify the transceiver from which the echo UWB pulse is emitted. Therefore, target information in the radar coverage area can be extracted via single-channel cooperative signal processing in the CO. In addition,

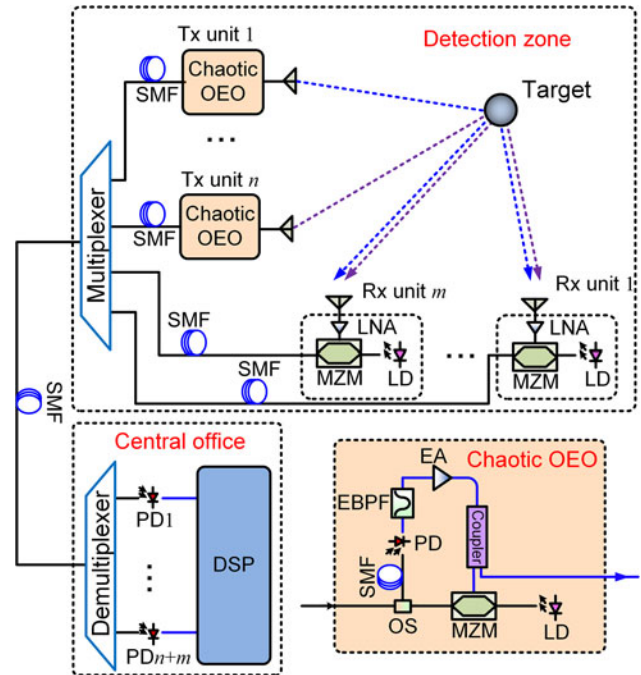


Fig. 24. Distributed MIMO chaotic radar based on WDM technology. OS: optical splitter. EBPF: electrical bandpass filter. EA: electrical amplifier.

wavelength-reuse is applied in each transceiver to simplify the system and polarization division multiplexing is employed to avoid optical interference. Experiments have shown that 2-D localization with centimeter-level accuracy is achievable.

It is worth noting that the OTDM-based fiber-connected distributed radar requires ultrashort pulse sources to prevent signal overlap between different transceivers. In addition, the length of the SMF between the adjacent transceivers must be carefully selected according to the pulse repetition, pulse duration, transceivers separation, and detection zone. If the received signals are separated in the wavelength domain, both the pulsed and non-pulsed signal sources can be applied. In [96], a novel concept to realize a distributed MIMO chaotic radar that functions without complex signal processing and precise clock synchronization in each receiver was proposed and demonstrated based on WDM technology.

Fig. 24 shows the schematic diagram, where the wideband quasi-orthogonal chaotic signals are generated by chaotic OEOs with a bandwidth of 7.5 GHz. All of the reference signals from the transmitters and the received signals from the receivers are sent to the CO via a WDM network for joint signal processing. Two-dimensional localization of a metal target with a position error below 6.5 cm is realized.

IV. OTHER PHOTONICS-BASED MICROWAVE MEASUREMENT TECHNIQUES

In addition to those discussed above, emerging photonic techniques have opened up many other possibilities and capacities in broadband microwave measurement, such as microwave passive direction finding, Doppler frequency shift estimation, and multi-antenna based GPS positioning.

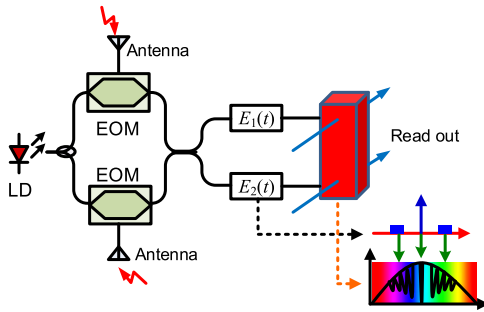


Fig. 25. DOA estimation system based on SHB effect.

A. Microwave Passive Direction Finding

Direction-of-arrival (DOA) estimation can be used to minimize the signal power of the interference while maximizing the power of the desired signal, improving the performance of the system. Therefore, DOA is a very interesting capability for broadband mobile systems and electronic warfare systems. Several interesting approaches have been proposed for direction finding of microwave signals [97]–[99].

In arrayed antennas, the incoming signal at each antenna arrives with a different time delay depending on the angle between the signal source and the antenna array. By measuring the relative time delay, the angle of incidence can be calculated accordingly. Till now, photonics-based DOA can be achieved based on phase shift to power mapping and SHB in spatial-spectral materials.

Phase shift to power mapping based DOA measurement system can be achieved by two cascaded EOMs with optical CS-DSB modulation [98]. Because of the phase difference between the two received RF signals, the total power at the carrier wavelength will be a function of the phase shift, thus, by detecting the power at the carrier wavelength, the phase shift can be estimated and the DOA can be calculated accordingly.

Fig. 25 shows a diagram of a typical DOA estimation system based on SHB effect in spatial-spectral materials [99]. The microwave signals are modulated on an optical carrier at two parallel modulators, then the obtained optical microwave signals are combined by an optical coupler where they interfere with each other. Two optical signals are achieved at the two output ports of the optical coupler, each of which consists of an upper sideband, optical carrier, and a lower sideband. The spectra of the two signals are recorded at different positions in the spatial-spectral material by SHB effect. The depths of the spectral holes is dependent on the powers of the optical spectral components. Then, the recorded upper (or lower) sidebands of both optical signals are read out by two chirped laser beams. The power ratio of the two upper (or lower) sidebands can be used to calculate the time difference of arrival and the DOA.

B. Doppler Frequency Shift Estimation

Doppler frequency shift widely exists in applications such as wireless communications, electronic warfare, and radars. Quantitatively and accurately Doppler frequency shift measurement within a wide frequency range is thus required.

Using a photonics-based technique shown in Fig. 26, the Doppler frequency shift can be measured with a high resolu-

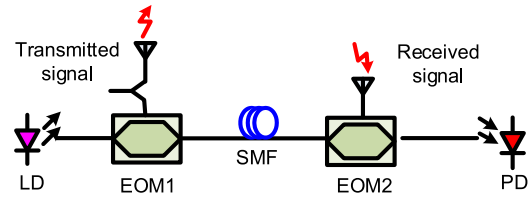


Fig. 26. Photonic Doppler frequency shift estimation system.

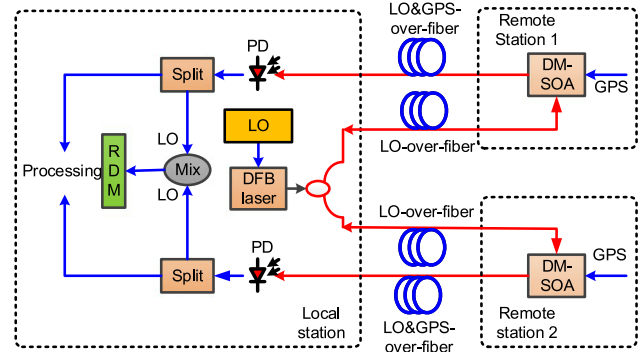


Fig. 27. Diagram of a typical multi-antenna based GPS positioning system. DM-SOA: directly modulated semiconductor optical amplifier. RDM: relative delay monitor.

tion and a wide frequency range. The original microwave signal before emitting is modulated on an optical carrier using EOM1 with optical CS-DSB modulation, while the received microwave signal with Doppler frequency shift is launched into EOM2, performing DSB with carrier modulation. Using a low-speed PD, the Doppler frequency shift can be obtained. In a previous study, a measurement range from -90 to 90 kHz with a measurement error within $\pm 5 \times 10^{-10}$ Hz was achieved [100].

C. Multi-Antenna Receiver-Based GPS Positioning

Multi-antenna receiver based GPS positioning systems have been developed for attitude determination as well as deformation monitoring of engineering structures [101], [102]. By using only one receiver while transmitting the GPS signal from the antennas to the receiver via optical fiber, the well-known limitation of conventional systems, i.e. the error in the vertical is two to three times than that in the horizontal due to the inhomogeneity of the satellite sky distribution and the receiver clock errors can be possibly solved. Such type of system is depicted in Fig. 27 [103]. A distributed feedback laser in the local station is directly modulated by a LO signal to produce an optical reference signal, then the optical signals are then divided into two paths and sent via optical fibers to two directly-modulated semiconductor optical amplifiers in the remote stations. In the semiconductor optical amplifiers, the LO carried in the optical signal mixes with the GPS signals received by the antennas, downconverting the GPS signals to IF signals. The modulated GPS-IF signals in tandem with the reference signals are then transmitted back to the local station and converted back to the electrical signals. By measuring the phase difference between the two received LOs, the relative delay of the two paths can be estimated. With this relative delay, high vertical precision can be guaranteed by certain algorithm. Since there is only one receiver in the local

station, the relative clock errors are preventable. As a result, mm-level measurement resolution can be obtained along both vertical and horizontal axes.

V. DISCUSSIONS AND CONCLUSION

This paper provided an overview of the photonics-based technologies developed over the past two decades for the acquisition of microwave signal parameters and the non-contact measurement of object properties, with an emphasis on relevant principles and system architectures for measuring electromagnetic fields, phase noise, instantaneous frequencies and spectra. Photonics-based radar systems, fiber-connected distributed antenna systems, and a few emerging topics in this area (e.g., passive direction finding, Doppler frequency shift measurement and multi-antenna-based GPS positioning) were also reviewed.

Although some of the photonics-based microwave measurement systems discussed here have been commercialized, such as the electric-field measurement and the phase noise measurement system, most remain merely conceptual due to the relative immaturity of photonic-based techniques for microwave applications in general. The primary performance limitation factors are the high noise figure of the systems due to low electrical-to-optical or optical-to-electrical conversion efficiency, the relatively small dynamic range because of the nonlinearity of the EOMs and the low power handling capability of the PDs. These problems could be overcome by post signal processing such as long-term averaging, multiple-channel measurement with data fusion or advanced algorithms, so the trend that an increasing number of photonic techniques are being applied for microwave measurement is clear. In addition, rapid development in photonics integrated circuits may soon result in ultra-compact and reliable photonics-based microwave measurement solutions with significantly improved performance.

ACKNOWLEDGMENT

The author would like to thank several individuals from the Key Laboratory of Radar Imaging and Microwave Photonics, Ministry of Education, Nanjing University of Aeronautics and Astronautics, Nanjing, China, for their assistance: X. Wang, F. Zhang, Z. Tang, J. Shi, X. Ye, X. Chen, M. Xue, J. Fu, and W. Xu.

REFERENCES

- [1] J. Yao, "Microwave photonics," *J. Lightw. Technol.*, vol. 27, no. 3, pp. 314–335, Feb. 2009.
- [2] J. Capmany, J. Mora, I. Gasulla, J. Sancho, J. Lloret, and S. Sales, "Microwave photonic signal processing," *J. Lightw. Technol.*, vol. 31, no. 4, pp. 571–586, Feb. 2013.
- [3] D. Marpaung, C. Roeloffzen, R. Heideman, A. Leinse, S. Sales, and J. Capmany, "Integrated microwave photonics," *Laser Photon. Rev.*, vol. 7, no. 4, pp. 506–538, Jul. 2013.
- [4] S. Pan, D. Zhu, and F. Zhang, "Microwave photonics for modern radar systems," *Trans. Nanjing Univ. Aeronaut. Astronaut.*, vol. 3, no. 3, pp. 219–240, Jun. 2014.
- [5] S. Pan *et al.*, "Satellite payloads pay off," *IEEE Microw. Mag.*, vol. 16, no. 8, pp. 61–73, Sep. 2015.
- [6] R. A. Minasian, "Ultra-wideband and adaptive photonic signal processing of microwave signals," *IEEE J. Quantum Electron.*, vol. 52, no. 1, pp. 1–13, Jan. 2016.
- [7] W. D. Prather, C. E. Baum, R. J. Torres, F. Sabath, and D. Nitsch, "Survey of worldwide high-power wideband capabilities," *IEEE Trans. Electromagn. Compat.*, vol. 46, no. 3, pp. 335–344, Aug. 2004.
- [8] K. Yang, G. David, J.-G. Yook, I. Papapolymerou, L. P. Katehi, and J. F. Whitaker, "Electrooptic mapping and finite-element modeling of the near-field pattern of a microstrip patch antenna," *IEEE Trans. Microw. Theory Techn.*, vol. 48, no. 2, pp. 288–294, Feb. 2000.
- [9] X. Zhang *et al.*, "Electro-optic polymer infiltrated silicon slot photonic crystal waveguide for broadband electromagnetic field sensing," presented at the Integrated Photonics Research, Silicon Nanophotonics, San Diego, CA, USA, 2014, Paper IW2A. 3.
- [10] L. Duvillearet, S. Rialland, and J.-L. Coutaz, "Electro-optic sensors for electric field measurements. I. Theoretical comparison among different modulation techniques," *J. Opt. Soc. Amer. B*, vol. 19, no. 11, pp. 2692–2703, Nov. 2002.
- [11] L. Duvillearet, S. Rialland, and J.-L. Coutaz, "Electro-optic sensors for electric field measurements. II. Choice of the crystals and complete optimization of their orientation," *J. Opt. Soc. Amer. B*, vol. 19, no. 11, pp. 2704–2715, Nov. 2002.
- [12] Q. Yang, S. Sun, R. Han, W. Sima, and T. Liu, "Intense transient electric field sensor based on the electro-optic effect of LiNbO₃," *AIP Adv.*, vol. 5, no. 10, Oct. 2015, Art. no. 107130.
- [13] J. Santos-Aguilar and C. Gutiérrez-Martínez, "Lithium Niobate (LiNbO₃) optical retarders used as electric field sensors," in *Proc. 7th Int. Conf. Sensing Technol.*, 2013, pp. 660–664.
- [14] K. Yang, L. Katehi, and J. Whitaker, "Electro-optic field mapping system utilizing external gallium arsenide probes," *Appl. Phys. Lett.*, vol. 77, no. 4, pp. 486–488, Jul. 2000.
- [15] G. Gaborit, P. Jarrige, J. Dahdah, L. Gillette, and L. Duvillearet, "Packaged optical sensors for the electric field characterization in harsh environments," in *Proc. Int. Conf. Electromagn. Adv. Appl.*, 2015, pp. 1468–1471.
- [16] G. Gaborit *et al.*, "A nonperturbative electrooptic sensor for in situ electric discharge characterization," *IEEE Trans. Plasma Sci.*, vol. 41, no. 10, pp. 2851–2857, Oct. 2013.
- [17] R. Zeng, B. Wang, Z. Yu, and W. Chen, "Design and application of an integrated electro-optic sensor for intensive electric field measurement," *IEEE Trans. Dielectr. Electr. Insul.*, vol. 18, no. 1, pp. 312–319, Feb. 2011.
- [18] Q. Wu and X.-C. Zhang, "7 terahertz broadband GaP electro-optic sensor," *Appl. Phys. Lett.*, vol. 70, no. 14, pp. 1784–1786, Jan. 1997.
- [19] A. Nahata, A. S. Weling, and T. F. Heinz, "A wideband coherent terahertz spectroscopy system using optical rectification and electro-optic sampling," *Appl. Phys. Lett.*, vol. 69, no. 16, pp. 2321–2323, Aug. 1996.
- [20] H. Liu, C. Song, A. SpringThorpe, and J. Cao, "Terahertz quantum-well photodetector," *Appl. Phys. Lett.*, vol. 84, no. 20, pp. 4068–4070, May 2004.
- [21] B. J. Gouhier, L. Ka-Lun, A. Nirmalathas, L. Christina, and E. Skafidas, "Recirculating frequency shifter-based hybrid electro-optic probing system with ultra-wide bandwidth," *IEICE Trans. Electron.*, vol. 98, no. 8, pp. 857–865, Aug. 2015.
- [22] D.-J. Lee and J. F. Whitaker, "Bandwidth enhancement of electro-optic sensing using high-even-order harmonic sidebands," *Opt. Express*, vol. 17, no. 17, pp. 14909–14917, Aug. 2009.
- [23] X. Zhang *et al.*, "Integrated photonic electromagnetic field sensor based on broadband bowtie antenna coupled silicon organic hybrid modulator," *J. Lightw. Technol.*, vol. 32, no. 20, pp. 3774–3784, Oct. 2014.
- [24] C. Volat, M. Jabbari, M. Farzaneh, and L. Duvillearet, "New method for in live-line detection of small defects in composite insulator based on electro-optic E-field sensor," *IEEE Trans. Dielectr. Electr. Insul.*, vol. 20, no. 1, pp. 194–201, Feb. 2013.
- [25] A. G. Armada and M. Calvo, "Phase noise and sub-carrier spacing effects on the performance of an OFDM communication system," *IEEE Commun. Lett.*, vol. 2, no. 1, pp. 11–13, Jan. 1998.
- [26] D. K. Barton, *Radar System Analysis and Modeling*. Norwood, MA, USA: Artech House, 2004.
- [27] B. Brannon, "Sampled systems and the effects of clock phase noise and jitter," *Analog Devices App. Note*, vol. AN-756, pp. 1–11, 2004.
- [28] U. L. Rohde, A. K. Poddar, and A. M. Apte, "Getting its measure: Oscillator phase noise measurement techniques and limitations," *IEEE Microw. Mag.*, vol. 14, no. 6, pp. 73–86, Oct. 2013.
- [29] C. Schiebold, "Theory and design of the delay line discriminator for phase noise measurements," *Microw. J.*, vol. 26, no. 12, pp. 102–112, 1983.
- [30] PN9000 Phase Noise Test System. (2016). [Online]. Available: http://www.noisext.com/index.php?option=com_content&view=article&id=58&Itemid=194

- [31] E. Rubiola, E. Salik, S. Huang, N. Yu, and L. Maleki, "Photonic-delay technique for phase-noise measurement of microwave oscillators," *J. Opt. Soc. Amer. B*, vol. 22, no. 5, pp. 987–997, May 2005.
- [32] K. Volyanskiy *et al.*, "Applications of the optical fiber to the generation and measurement of low-phase-noise microwave signals," *J. Opt. Soc. Amer. B*, vol. 25, no. 12, pp. 2140–2150, Dec. 2008.
- [33] D. Zhu, F. Zhang, P. Zhou, D. Zhu, and S. Pan, "Wideband phase noise measurement using a multifunctional microwave photonic processor," *IEEE Photon. Technol. Lett.*, vol. 26, no. 24, pp. 2434–2437, Dec. 2014.
- [34] S. Pan and Y. Zhang, "Tunable and wideband microwave photonic phase shifter based on a single-sideband polarization modulator and a polarizer," *Opt. Lett.*, vol. 37, no. 21, pp. 4483–4485, Nov. 2012.
- [35] D. Zhu, F. Zhang, P. Zhou, and S. Pan, "Phase noise measurement of wideband microwave sources based on a microwave photonic frequency down-converter," *Opt. Lett.*, vol. 40, no. 7, pp. 1326–1329, Apr. 2015.
- [36] J. Zhang, H. Chen, M. Chen, T. Wang, and S. Xie, "A photonic microwave frequency quadrupler using two cascaded intensity modulators with repetitious optical carrier suppression," *IEEE Photon. Technol. Lett.*, vol. 19, no. 14, pp. 1057–1059, Jul. 2007.
- [37] F. Zhang, D. Zhu, and S. Pan, "Photonic-assisted wideband phase noise measurement of microwave signal sources," *Electron. Lett.*, vol. 51, no. 16, pp. 1272–1274, Aug. 2015.
- [38] R. Vessot, L. Mueller, and J. Vanier, "A cross-correlation technique for measuring the short-term properties of stable oscillators," Short-Term Frequency Stability, NASA SP-80, Washington, DC, USA, 1965, p. 111.
- [39] E. Salik, N. Yu, L. Maleki, and E. Rubiola, "Dual photonic-delay line cross correlation method for phase noise measurement," in *Proc. IEEE Int. Proc. Freq. Control Symp. Expo.*, 2004, pp. 303–306.
- [40] P. Salzenstein *et al.*, "Realization of a phase noise measurement bench using cross correlation and double optical delay line," *Acta Phys. Pol. Series a*, vol. 112, no. 5, pp. 1107–1111, Sep. 2007.
- [41] PHENOMTM phase noise measurement system. (2016). [Online]. Available: <http://www.oewaves.com/phase-noise-measurement>
- [42] S. Pan and J. Yao, *Photonics-Assisted Instantaneous Frequency Measurement*. Hoboken, NJ, USA: Wiley, 2012.
- [43] J. M. Heaton *et al.*, "16-channel (1-to 16-GHz) microwave spectrum analyzer device based on a phased array of GaAs/AlGaAs electro-optic waveguide delay lines," in *Proc. Optoelectron. High-Power Lasers Appl.*, 1998, pp. 245–251.
- [44] W. Wang *et al.*, "Characterization of a coherent optical RF channelizer based on a diffraction grating," *IEEE Trans. Microw. Theory Techn.*, vol. 49, no. 10, pp. 1996–2001, Oct. 2001.
- [45] D. Hunter, L. Edvell, and M. Englund, "Wideband microwave photonic channelised receiver," in *Proc. Int. Top. Meet. Microw. Photon.*, 2005, pp. 249–252.
- [46] S. T. Winnall, A. Lindsay, M. W. Austin, J. Canning, and A. Mitchell, "A microwave channelizer and spectroscopy based on an integrated optical Bragg-grating Fabry-Perot and integrated hybrid Fresnel lens system," *IEEE Trans. Microw. Theory Techn.*, vol. 54, no. 2, pp. 868–872, Feb. 2006.
- [47] R. K. Mohan *et al.*, "Ultra-wideband spectral analysis using S2 technology," *J. Lumin.*, vol. 127, no. 1, pp. 116–128, Nov. 2007.
- [48] G. Gorju, V. Crozatier, I. Lorigeré, J. Le Gouët, and F. Bretenaker, "10-GHz bandwidth RF spectral analyzer with MHz resolution based on spectral hole burning in Tm³⁺: YAG," *IEEE Photon. Technol. Lett.*, vol. 17, no. 11, pp. 2385–2387, Nov. 2005.
- [49] F. Schlottau, M. Colice, K. Wagner, and W. R. Babbitt, "Spectral hole burning for wideband, high-resolution radio-frequency spectrum analysis," *Opt. Lett.*, vol. 30, no. 22, pp. 3003–3005, Nov. 2005.
- [50] X. J. Xie *et al.*, "Broadband photonic radio-frequency channelization based on a 39-GHz optical frequency comb," *IEEE Photon. Technol. Lett.*, vol. 24, no. 8, pp. 661–663, Apr. 2012.
- [51] Y. Dai, K. Xu, X. Xie, L. Yan, R. Wang, and J. Lin, "Broadband photonic radio frequency (RF) channelization based on coherent optical frequency combs and polarization IQ demodulation," *Sci. China Technol. Sc.*, vol. 56, no. 3, pp. 621–628, Jan. 2013.
- [52] W. Xu, D. Zhu, and ShilongPan, "Coherent photonic RF channelization based on dual coherent optical frequency combs and stimulated Brillouin scattering," *Opt. Eng.*, vol. 55, no. 4, Apr. 2016, Art no. 046106.
- [53] L. Ménager, I. Lorigeré, J.-L. Le Gouët, D. Dolfi, and J.-P. Huignard, "Demonstration of a radio-frequency spectrum analyzer based on spectral hole burning," *Opt. Lett.*, vol. 26, no. 16, pp. 1245–1247, Aug. 2001.
- [54] M. Colice, F. Schlottau, and K. H. Wagner, "Broadband radio-frequency spectrum analysis in spectral-hole-burning media," *Appl. Opt.*, vol. 45, no. 25, pp. 6393–6408, 2006.
- [55] M. Colice, J. Xiong, and K. H. Wagner, "Frequency-doubled fiber lasers for RF spectrum analysis in spectral-hole-burning media," *IEEE J. Quantum Electron.*, vol. 44, no. 6, pp. 587–594, Jun. 2008.
- [56] V. Lavielle, I. Lorigeré, J.-L. Le Gouët, S. Tonda, and D. Dolfi, "Wideband versatile radio-frequency spectrum analyzer," *Opt. Lett.*, vol. 28, no. 6, pp. 384–386, Mar. 2003.
- [57] L. V. Nguyen and D. B. Hunter, "A photonic technique for microwave frequency measurement," *IEEE Photon. Technol. Lett.*, vol. 18, no. 9–12, pp. 1188–1190, May 2006.
- [58] X. Zou and J. Yao, "An optical approach to microwave frequency measurement with adjustable measurement range and resolution," *IEEE Photon. Technol. Lett.*, vol. 20, no. 23, pp. 1989–1991, Dec. 2008.
- [59] X. Zhang, H. Chi, X. Zhang, S. Zheng, X. Jin, and J. Yao, "Instantaneous microwave frequency measurement using an optical phase modulator," *IEEE Microw. Wireless Compon. Lett.*, vol. 19, no. 6, pp. 422–424, Jun. 2009.
- [60] M. Attygalle and D. B. Hunter, "Improved photonic technique for broadband radio-frequency measurement," *IEEE Photon. Technol. Lett.*, vol. 21, no. 4, pp. 206–208, Feb. 2009.
- [61] X. Zou, S. Pan, and J. Yao, "Instantaneous microwave frequency measurement with improved measurement range and resolution based on simultaneous phase modulation and intensity modulation," *J. Lightw. Technol.*, vol. 27, no. 23, pp. 5314–5320, Dec. 2009.
- [62] J. Zhou, S. Fu, S. Aditya, P. P. Shum, and C. Lin, "Instantaneous microwave frequency measurement using photonic technique," *IEEE Photon. Technol. Lett.*, vol. 21, no. 15, pp. 1069–1071, Aug. 2009.
- [63] S. Pan and J. Yao, "Instantaneous microwave frequency measurement using a photonic microwave filter pair," *IEEE Photon. Technol. Lett.*, vol. 22, no. 19, pp. 1437–1439, Oct. 2010.
- [64] H. Y. Fu, Z. W. Xu, and K. Zhu, "Remote wideband microwave frequency measurement based on a single-passband microwave photonic filter," *IEEE Photon. J.*, vol. 4, no. 5, pp. 1401–1406, Oct. 2012.
- [65] N. N. Shi, Y. Y. Gu, J. J. Hu, Z. J. Kang, X. Y. Han, and M. S. Zhao, "Photonic approach to broadband instantaneous microwave frequency measurement with improved accuracy," *Opt. Commun.*, vol. 328, pp. 87–90, Oct. 2014.
- [66] Y. Q. Li, L. Pei, J. Li, Y. Q. Wang, and J. Yuan, "Theory study on a range-extended and resolution-improved microwave frequency measurement," *J. Mod. Opt.*, vol. 63, no. 7, pp. 613–620, Sep. 2015.
- [67] H. Emami and M. Ashourian, "Improved dynamic range microwave photonic instantaneous frequency measurement based on four-wave mixing," *IEEE Trans. Microw. Theory Techn.*, vol. 62, no. 10, pp. 2462–2470, Oct. 2014.
- [68] Z. Li, C. Wang, M. Li, H. Chi, X. Zhang, and J. Yao, "Instantaneous microwave frequency measurement using a special fiber Bragg grating," *IEEE Microw. Wireless Compon. Lett.*, vol. 21, no. 1, pp. 52–54, Jan. 2011.
- [69] H. Guo, G. Xiao, N. Mrad, and J. Yao, "Measurement of microwave frequency using a monolithically integrated scannable echelle diffractive grating," *IEEE Photon. Technol. Lett.*, vol. 21, no. 1, pp. 45–47, Jan. 2009.
- [70] H. Emami, N. Sarkhosh, L. A. Bui, and A. Mitchell, "Wideband RF photonic in-phase and quadrature-phase generation," *Opt. Lett.*, vol. 33, no. 2, pp. 98–100, Jan. 2008.
- [71] L. V. Nguyen, "Microwave photonic technique for frequency measurement of simultaneous signals," *IEEE Photon. Technol. Lett.*, vol. 21, no. 10, pp. 642–644, May 2009.
- [72] T. A. Nguyen, E. H. W. Chan, and R. A. Minasian, "Instantaneous high-resolution multiple-frequency measurement system based on frequency-to-time mapping technique," *Opt. Lett.*, vol. 39, no. 8, pp. 2419–2422, Apr. 2014.
- [73] D. R. Reilly, S. X. Wang, and G. S. Kanter, "Nonuniform optical undersampling for high-resolution microwave frequency measurements," *IEEE Photon. Technol. Lett.*, vol. 24, no. 12, pp. 997–999, Jun. 2012.
- [74] H. Chi, X. Zou, and J. Yao, "An approach to the measurement of microwave frequency based on optical power monitoring," *IEEE Photon. Technol. Lett.*, vol. 20, no. 14, pp. 1249–1251, Jul. 2008.
- [75] J. S. Fandiño and P. Muñoz, "Photonics-based microwave frequency measurement using a double-sideband suppressed-carrier modulation and an InP integrated ring-assisted Mach-Zehnder interferometer filter," *Opt. Lett.*, vol. 38, no. 21, pp. 4316–4319, Nov. 2013.

- [76] D. Q. Feng, H. Xie, L. F. Qian, Q. H. Bai, and J. Q. Sun, "Photonic approach for microwave frequency measurement with adjustable measurement range and resolution using birefringence effect in highly non-linear fiber," *Opt. Express*, vol. 23, no. 13, pp. 17613–17621, Jun. 2015.
- [77] L. Liu *et al.*, "Photonic measurement of microwave frequency using a silicon microdisk resonator," *Opt. Commun.*, vol. 335, pp. 266–270, Jan. 2015.
- [78] M. Pagani *et al.*, "Low-error and broadband microwave frequency measurement in a silicon chip," *Optica*, vol. 2, no. 8, pp. 751–756, Aug. 2015.
- [79] T. A. Nguyen, E. H. W. Chan, and R. A. Minasian, "Photonic multiple frequency measurement using a frequency shifting recirculating delay line structure," *J. Lightw. Technol.*, vol. 32, no. 20, pp. 3831–3838, Oct. 2014.
- [80] D. Marpaung, "On-chip photonic-assisted instantaneous microwave frequency measurement system," *IEEE Photon. Technol. Lett.*, vol. 25, no. 9, pp. 837–840, May 2013.
- [81] H. Y. Jiang *et al.*, "Wide-range, high-precision multiple microwave frequency measurement using a chip-based photonic Brillouin filter," *Optica*, vol. 3, no. 1, pp. 30–34, Jan. 2016.
- [82] M. Skolnik, *Radar Handbook*. New York, NY, USA: McGraw-Hill, 2008.
- [83] P. Ghelfi *et al.*, "A fully photonics-based coherent radar system," *Nature*, vol. 507, no. 7492, pp. 341–345, Mar. 2014.
- [84] F. Scotti, F. Laghezza, P. Ghelfi, and A. Bogoni, "Multi-band software-defined coherent radar based on a single photonic transceiver," *IEEE Trans. Microw. Theory Techn.*, vol. 63, no. 2, pp. 546–552, Feb. 2015.
- [85] F. Scotti, D. Onori, and F. Laghezza, "Fully coherent S-and X-band photonics-aided radar system demonstration," *IEEE Microw. Wireless Compon. Lett.*, vol. 25, no. 11, pp. 757–759, Nov. 2015.
- [86] P. Ghelfi, F. Laghezza, F. Scotti, and D. Onori, "Photonics for radars operating on multiple coherent bands," *J. Lightw. Technol.*, vol. 34, no. 2, pp. 500–507, Jan. 2016.
- [87] W. Zou, H. Zhang, X. Long, S. Zhang, Y. Cui, and J. Chen, "All-optical central-frequency-programmable and bandwidth-tailorable radar," *Sci. Rep.*, vol. 6, Jan. 2016, Art. no. 19786.
- [88] V. S. Chernyak, *Fundamentals of Multisite Radar Systems: Multistatic Radars and Multistatic Radar Systems*. Boca Raton, FL, USA: CRC Press, 1998.
- [89] C. Baker, A. Hume, and C. J. Baker, "Netted radar sensing," *IEEE Aerosp. Electron. Syst. Mag.*, vol. 18, no. 2, pp. 3–6, Feb. 2003.
- [90] A. M. Haimovich, R. S. Blum, and L. J. Cimini, "MIMO radar with widely separated antennas," *IEEE Signal Process. Mag.*, vol. 25, no. 1, pp. 116–129, 2008.
- [91] Y. Xu, S. Wu, J. Shao, J. Chen, and G. Fang, "Life detection and location by MIMO ultra wideband radar," in *Proc. 14th Int. Conf. Ground Penetrating Radar*, 2012.
- [92] R. Thomä, O. Hirsch, J. Sachs, and R. Zetik, *UWB Sensor Networks for Position Location and Imaging of Objects and Environments*. Hoboken, NJ, USA: Wiley, 2009.
- [93] H. Al-Raweshidy and S. Komaki, *Radio Over Fiber Technologies for Mobile Communications Networks*. Norwood, MA, USA: Artech House, 2002.
- [94] S. Pan and J. Yao, "UWB-over-fiber communications: modulation and transmission," *J. Lightw. Technol.*, vol. 28, no. 16, pp. 2445–2455, Aug. 2010.
- [95] J. Fu and S. Pan, "A fiber-distributed bistatic ultra-wideband radar based on optical time division multiplexing," in *Proc. Int. Top. Meet. Microw. Photon.*, 2015, pp. 1–4.
- [96] T. Yao, D. Zhu, D. Ben, and S. Pan, "Distributed MIMO chaotic radar based on wavelength-division multiplexing technology," *Opt. Lett.*, vol. 40, no. 8, pp. 1631–1634, Apr. 2015.
- [97] B. Vidal, M. A. Piqueras, and J. Martí, "Direction-of-arrival estimation of broadband microwave signals in phased-array antennas using photonic techniques," *J. Lightw. Technol.*, vol. 24, no. 7, pp. 2741–2745, Jul. 2006.
- [98] X. Zou, W. Li, W. Pan, B. Luo, L. Yan, and J. Yao, "Photonic approach to the measurement of time-difference-of-arrival and angle-of-arrival of a microwave signal," *Opt. Lett.*, vol. 37, no. 4, pp. 755–757, Feb. 2012.
- [99] R. K. Mohan, C. Harrington, T. Sharpe, Z. W. Barber, and W. R. Babbitt, "Broadband multi-emitter signal analysis and direction finding using a dual-port interferometric photonic spectrum analyzer based on spatial-spectral materials," in *Proc. Int. Top. Meet. Microw. Photon.*, 2013, pp. 241–244.
- [100] X. Zou, W. Li, B. Lu, W. Pan, L. Yan, and L. Shao, "Photonic approach to wide-frequency-range high-resolution microwave/millimeter-wave Doppler frequency shift estimation," *IEEE Trans. Microw. Theory Techn.*, vol. 63, no. 4, pp. 1421–1430, Apr. 2015.
- [101] G. R. Song Xixi, Z. Yonggang, and P. Shilong, "Experimental demonstration of a GPS-over-fiber multi-antenna receiver system," *J. Data Acquisition Process.*, vol. 06, pp. 957–963, 2014.
- [102] X. Ding, Y. Chen, D. Huang, J. Zhu, M. Tsakiri, and M. Stewart, "Slope monitoring using GPS: A multi-antenna approach," *GPS World*, vol. 11, no. 3, pp. 52–55, 2000.
- [103] D. Macias-Valadez, S. LaRochelle, R. Santerre, and B. Filion, "Fiber optic synchronisation architecture for high precision GPS applications," presented at the Optical Fiber Communication Conf., San Diego, CA, USA, 2009, Paper OWF6.

Shilong Pan (S'06–M'09–SM'13) received the B.S. and Ph.D. degrees in electronics engineering from Tsinghua University, Beijing, China, in 2004 and 2008, respectively. From 2008 to 2010, he was a "Vision 2010" Postdoctoral Research Fellow in the Microwave Photonics Research Laboratory, University of Ottawa, Canada. He joined the College of Electronic and Information Engineering, Nanjing University of Aeronautics and Astronautics, China, in 2010, where he is currently a Full Professor and the Executive Director of the Key Laboratory of Radar Imaging and Microwave Photonics (Nanjing Univ. Aeronaut. Astronaut.), Ministry of Education.

His research has focused on microwave photonics, which includes optical generation and processing of microwave signals, ultrawideband over fiber, photonic microwave measurement, and integrated microwave photonics. He has authored or co-authored more than 250 research papers, including more than 130 papers in peer-reviewed journals and 120 papers in conference proceedings.

Dr. Pan is a Senior Member of the IEEE Microwave Theory and Techniques Society, the IEEE Photonics Society, the IEEE Instrumentation and Measurement Society, and a Member of the Optical Society of America. He was selected to receive an OSA outstanding Reviewer Award in 2015. He is currently a Topical Editor for Chinese Optics Letters. He was the Chair of numerous international conferences and workshops, including the TPC Chair of the International Conference on Optical Communications and Networks in 2015, the TPC Chair of the high-speed and broadband wireless technologies subcommittee of the IEEE Radio Wireless Symposium in 2013, 2014, and 2016, the TPC Chair of the Optical fiber sensors and the microwave photonics subcommittee Chair of the OptoElectronics and Communication Conference in 2015, and the Chair of the microwave photonics for broadband measurement workshop of International Microwave Symposium in 2015.

Jianping Yao (M'99–SM'01–F'12) received the Ph.D. degree in electrical engineering from the Université de Toulon, Toulon, France, in December 1997.

He is a Professor and the University Research Chair at the School of Electrical Engineering and Computer Science, University of Ottawa, Ottawa. He joined the School of Electrical and Electronic Engineering, Nanyang Technological University, Singapore, as an Assistant Professor in 1998. In December 2001, he joined the School of Electrical Engineering and Computer Science, University of Ottawa, as an Assistant Professor, where he became an Associate Professor in 2003, and a Full Professor in 2006. He was appointed the University Research Chair in Microwave Photonics in 2007. From July 2007 to June 2010, he was the Director of the Ottawa-Carleton Institute for Electrical and Computer Engineering. He was reappointed as the Director of the Ottawa-Carleton Institute for Electrical and Computer Engineering in 2013. He has published more than 500 papers, including more than 290 papers in peer-reviewed journals and 210 papers in conference proceedings. He was a Guest Editor for the Focus Issue on Microwave Photonics in *Optics Express* in 2013 and a Feature Issue on Microwave Photonics in *Photonics Research* in 2014. He is currently a Topical Editor for *Optics Letters*, and serves on the Editorial Board of the IEEE TRANSACTIONS ON MICROWAVE THEORY AND TECHNIQUES, and *China Science Bulletin*.

Dr. Yao is the Chair of numerous international conferences, symposia, and workshops, including the Vice Technical Program Committee (TPC) Chair of the IEEE Microwave Photonics Conference in 2007, the TPC Cochair of the Asia-Pacific Microwave Photonics Conference in 2009 and 2010, the TPC Chair of the high-speed and broadband wireless technologies subcommittee of the IEEE Radio Wireless Symposium in 2009–2012, the TPC Chair of the microwave photonics subcommittee of the IEEE Photonics Society Annual Meeting in 2009, the TPC Chair of the IEEE Microwave Photonics Conference in 2010, the General Cochair of the IEEE Microwave Photonics Conference in 2011, the TPC Cochair of the IEEE Microwave Photonics Conference in 2014, and the General Cochair of the IEEE Microwave Photonics Conference in 2015. He received the 2005 International Creative Research Award at the University of Ottawa, the 2007 George S. Glinski Award for Excellence in Research, and the OSA Outstanding Reviewer Award in 2012. He is an IEEE MTT-S Distinguished Microwave Lecturer for 2013–2015. He is a registered Professional Engineer of Ontario. He is a Fellow of the Optical Society of America and the Canadian Academy of Engineering.